Universität Leipzig

Fakultät für Mathematik und Informatik
Institut für Informatik

Evolution of Moisture Transport Patterns in the North Atlantic in different Climate scenarios

Masterarbeit

Leipzig, Mai 2024

vorgelegt von

Denis Streitmatter
Studiengang Master Informatik

Betreuende Hochschullehrer:
Dr. Baldwin Nsonga
Universität Leipzig, Abteilung für Bild und Signalverarbeitung
Prof. Dr. Gerik Scheuermann
Universität Leipzig, Abteilung für Bild und Signalverarbeitung

Abstract

The distribution and variability of precipitation in Europe are significantly influenced by moisture transport over the north(east)ern Atlantic. The objective of my master thesis is to analyze the evolution of moisture transport patterns in various future climate scenarios. The foundation of this research lies in the MPI-GE, the Max Planck Institute Grand Ensemble Dataset, comprising an ensemble of 100 members for different RCP (climate) scenarios up until 2100. Each member provides multiple fields of relevant climate data. A challenge will be the visualization of uncertainty stemming from 100 different simulations, which will not be straightforward.

To quantify moisture transport, an integrated water vapor transport (a combination of wind and specific moisture) scalar/vector field will be generated from the MPI-GE. Windowed Empirical Orthogonal Functions (EOFs) will be used to extract spatial-temporal patterns and simplify the data, making it easier to evaluate pattern evolution over time.

Contents

1 Introduction and Motivation

1.1 Motivation

Since the discovery (and further confirmation) of the greenhouse effect in the years from 1824 to 1900 [9, 10] humans came a long way of fighting the consequences of the increased greenhouse gas concentration in earth's atmosphere. In 1972 Sawyer summarized the knwoledge and predicted quite accurately the warming at the end of the century [32]. Especially the last decades the climate crisis gained more and more attention, leading to the creation of multiple international organizations and institutions (e.g. the International Panel on Climate Change (IPCC) in 1988).

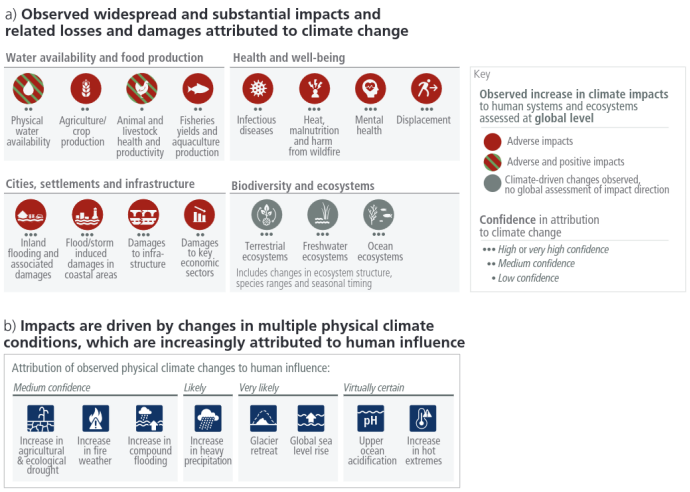

Figure 1.1: Impact of Climate Change for Humans, taken from [17]

In 2019 more than 11,000 scientists from around the world released a declaration [29], calling governments from around the world to action. The consequences for the environment and humans are prevalent and are, in part, already visible today. Figure 1.1 shows likely consequences for humans from the latest IPCC report for policy makers [17]: Flooding, malnutrition, displacement, and damages to all kinds of ecosystems can attributed with high confidence to climate change. The sources of such consequences are manyfold,

but recent research shows that big circulation systems like the North Atlantic Oscillation[39] or the Atlantic Meridional Overturning Circulation [19] change aswell.

Although the water vapor in the air accounts for only 0.001 % of the water on the earth, it is the most active part of that cycle [46]. Also reaserch shows that the preciptation on land does not match the evaporation, meaning the water was transported (from the oceans) to land, providing water for the ecosystems there. Analysing the structural change of this moisture transport could help predicting consequences. Motivated by the research of Vietinghoff et al., this thesis aims to evaluate in a similar manner the systemic changes of moisture transport patterns in Europe and the northern Atlantic.

CITE!!! Where the fuck did I read this?

1.2 Climate and Climate Research

1.2.1 Quick Overview over Climate Systems and Climate Change

Earth's climate system can be seen as complex interactions of its major components: atmosphere, hydrosphere, cryosphere, litho- sphere, and biosphere [14, 38]. Changes in this system can have (roughly) two reasons: Either "internal variations in form of redistributions of energy" [38], which can happen on arbitrary scales (see the discussion on the change of AMOC in [19]) or in the form of external forcings. Such forcings could be vulcanic activity, differences in solar radiation, and of course the emission of greenhouse gases (GHGs).

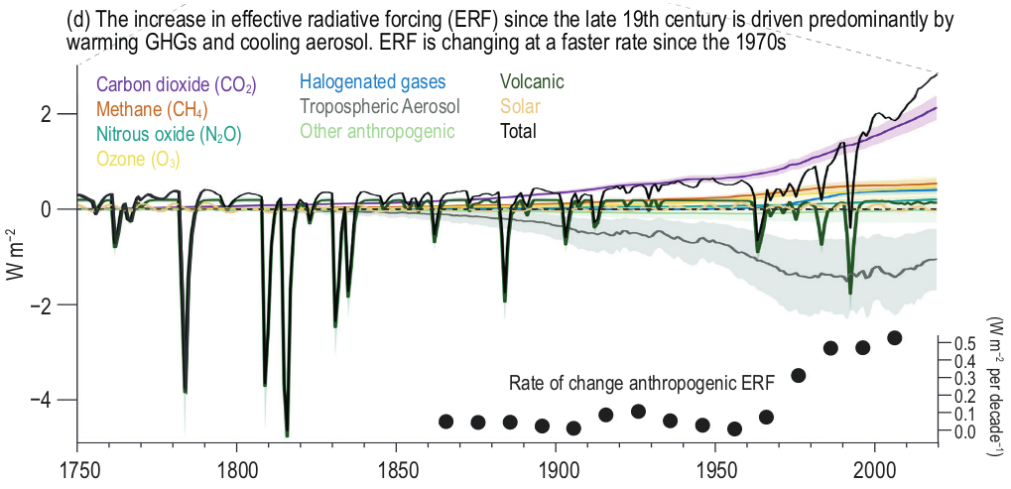

Figure 1.2: The evolution of the effective radiative forcing and contributing components, taken from [14]

Figure 1.2 gives an example what effect such external forcing can have: It shows the change in effective radiative forcing (ERF) and its contributing components. ERF (measured in Wm^{-2}) is a way of measuring how much energy from the sun is "trapped" instead of reflected back to space (greenhouse effect). A positive value means warming, while a negative value is associated with cooling. In can be seen in Figure 1.2 that neither volcanic activity or solar radiotian changed that much, the main drivers of change in ERF are the man-made GHGs and cooling aerosols. [14]

Regarding the internal variations: Most of it is part of some oscillation

1.2.2 Climate Research: The IPCC and the Coupled Model Intercomparison Project (CMIP)

The reason for the endorsement of the IPCC by the UN General Assembly 1988 was to prepare comprehensive reviews and report about the current state of scientific knowledge and research. Since then there were six assement cycles and six reports were published, condensing the research of the scientific community. Figure 1.1 is a graphic from the latest report for policy makers from 2023 [17], displaying the probable consequences for humans in climate change.

A main source for such figures in the reports are so-called Global Coupled Models (GCMs)[1], trying to model the state and evolution of certain fields of earth data. They consist of multiple Models, each representing a major part of Earth's complex climate system (like atmosphere, hydrosphere, etc.), also allowing to model the dynamic interactions between these parts [38]. In the mid 90s the Coupled Model Intercomparison Project (CMIP) was brought to life, with the aim of streamlining results of GCMs and making them compareable. CMIP provides the outer structure, amongst others what kind of simulations to produce (e.g. preindustrial control simulations, future scenarios etc.), what kinds of fields should be generated, what kind of resolutions to provide and also how these results should be serialized. Since then the results of CMIP played an increasingly major part in the reports of the IPCC [37], and are now even called "... one of the foundational elements of climate science" [7]. CMIP is currently in its 6th phase, corresponding to the recently finished 6th Assessment Report of the IPCC [17].

1.3 Research Questions and Thesis Structure

Following up the previous sections, the reasearch question for this thesis is:

[1] Unfortunately, Global Coupled Models share their acronym with General Circulation Models, which are quite similar

"How do the Patterns of Moisture Transport change in the face of various climate scenarios in the North-East Atlantic?"

The remaining thesis is structured as follows: Chapter 2 gives the theoretical background on fields and pattern analysis. The following Chapter 3 gives a detailed overview about the used CMIP6 based dataset. Chapter 4 provides an overview of related work, the motivation for this thesis and the placement of this thesis in the academic context. While the results are discussed and presented in Chapter 6, Chapter 5 gives a detailed description how these results came about. The thesis is concluded with Chapter 7 and gives an outlook for future research.

2 Basics

This section should explain the basic math to understand the aforementioned topics, not that much needed but still needs to be there.

2.1 (Uncertain) Fields

2.2 Empirical Orthogonal Functions

3 MPI GE CMIP6

The dataset chosen for this project is the *Max Planck Institute Grand Ensemble CMIP6* (from now on MPI-GE CMIP6), presented by Olonscheck et al. It is a Single-model initial-condition large ensemble (in short: SMILE) consisting of multiple coupled models: ECHAM6 for the atmosphere directly coupled to JSBACH for land and MPIOM for sea and sea-ice. The models are coupled once a day, meaning that the simulation results serve as inputs for the other models. This means that a single model was run with different initial conditions but the same external forcings (e.g. greenhous gasses) mutiple times. Every seperate intial condition is a member of the simulation, and all members together are the whole ensemble. [26]

Following this, every variable/field of the dataset can be interpreted as a uncertain field (see Section 2.1). Combining the members into an ensemble makes it possible to seperate the internal variability from the responses to the external forcing, enabling researchers to better quantify the consequences of climate change (for example). Additionally it makes the research of extreme weather phenomena (e.g. droughts, floods etc.) more robust in spite of their rare occurences [21].

Since MPI GE CMIP6 follows the CMIP6 protocol (see Section 1.2 and [7]), it implements the DECK core with (amongst others) a quasi-stationary preindustrial control simulation and the historical simulations. Futhermore it also uses the forcings defined by CMIP6 (like volcanic eruptions, solar circle etc.) for the historical and future simulations (see Section 3.1).

The historical simulations are split from 1000 year preindustrial control simulation circa 25 years apart for each member, and the results of them in the year 2015 serve as the initial state for each corresponding member in the future scenarios.

1. It uses the latest (6th) phase of the Coupled Model Intercomparison Project (CMIP6)

2. Compared to its predecessor (MPI-GE [22]) it provides high frequency output (6 hour intervals vs. monthly means), which enables taking short-lived weather events and structures (e.g. atmospheric rivers) into account which would be lost in the calculation of the mean

3.1 ScenarioMIP: Future Scenarios and Shared Socioeconomic Pathways

Since the goal of this thesis is to evaluate the future patterns of climate change, simulations of the future are necessary. Furtunately, CMIP (Phase 3) introduced a project of future climate scenarios (ScenarioMIP) in the 2000s, which define and simulate developments of different anthropogenic drivers of climate change [25]. They play an important role in climate research and are since then the source for many figures and assessments in IPCC reports [37]. The different scenarios can be used to assess "...possible changes in the climate system, impacts on society and ecosystems, and the effectiveness of response options such as adaptation and mitigation under a wide range of future outcomes" [25]. Basically, the differences between them are the forcings introduced by multiple variables, including change of land use, climate change mitigation policies, energy usage, population, economic growth and emissions [28]. For CMIP6 they extended the old model of RCPs (Representative Concentration Pathways), which were used for CMIP5, by adding so called Shared Socioeconomic Pathways (SSPs). These SSPs add socioeconomic reasons for the assumed changes in land use and emissions.

SSPs are derived from five broad, abstract narratives, which are then quantified in different ways. So for example the narrative for SSP1 is:

> "Sustainability – Taking the Green Road (Low challenges to mitigation and adaptation) The world shifts gradually, but pervasively, toward a more sustainable path, emphasizing more inclusive development that respects perceived environmental boundaries. Management of the global commons slowly improves, educational and health investments accelerate the demographic transition, and the emphasis on economic growth shifts toward a broader emphasis on human well-being. Driven by an increasing commitment to achieving development goals, inequality is reduced both across and within countries. Consumption is oriented toward low material growth and lower resource and energy intensity." [28]

while the narrative for SSP5 is:

> "Fossil-fueled Development – Taking the Highway (High challenges to mitigation, low challenges to adaptation) This world places increasing faith in competitive markets, innovation and participatory societies to produce rapid technological progress and development of human capital as the path to sustainable development. Global markets are increasingly integrated. There are also strong investments in health, education, and

institutions to enhance human and social capital. At the same time, the push for economic and social development is coupled with the exploitation of abundant fossil fuel resources and the adoption of resource and energy intensive lifestyles around the world. All these factors lead to rapid growth of the global economy, while global population peaks and declines in the 21st century. Local environmental problems like air pollution are successfully managed. There is faith in the ability to effectively manage social and ecological systems, including by geo-engineering if necessary." [28]

These narratives are then quantified in multiple dimensions (resource availability, technical development, lifestyle changes, population, economic activity etc.). These quantifications then serve as an input for a range of integrated assessment models (IAMs), which turn them into the actual forcings needed (e.g. land and energy use, emissions) [28].

In the actual scenarios these pathways are combined with the additional radiative forcing (RCP, the earlier version of scenarios in CMIP5), resulting in a matrix which can be seen in Figure 3.1. RCP describes the level of radiative forcing (in Wm^{-2}) reached in the year 2100 (see Section 1.2). Although there are now 35 possible scenarios, O'Neill et al. defined two different tiers of scenarios ranked by their importance. Figure 3.1 lists Tier 1, which are scenarios mostly compareable to the old RCP scenarios. These scenarios are available in the MPI GE CMIP6, amongst some of Tier 2. [3, 25, 28]

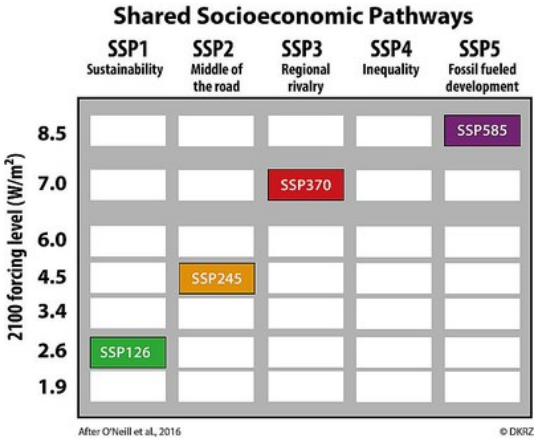

Figure 3.1: Combinations of SSPs and RCPs leading to scenarios compareable to the old RCPs [3]

3.2 Dataset description

3.2.1 Resolutions and Dimensions

In terms of spatial resolution, MPI GE CMIP6 comes in three variants: The low resolution variant MPI-ESM1.2-LR with a horizontal resolution of roughly 1.8° longitude/latitude resolution in the atmospheric part and 0.4° lon/lat for the ocean, the high resolution variant MPI-ESM1.2-HR with a horizontal resolution of 1.0°/0.4° for atmosphere/ocean and the extreme high resolution MPI-ESM1.2-XR with 0.5°/0.4° for atmosphere/ocean. Each variant has a vertical resolution of 47 levels for the atmosphere and 40 for ocean. With increasing spatial resolution comes decreased availability of other variables like simulation members, covered time period, and implemented scenarios. Although [26] reports 30 members for each simulation (for the LR variant), in the actual dataset available for this work 50 member were simulated.

In terms of time resolution, MPI GE CMIP6 provides very few, limited variables in 3 hour intervals and most variables in a 6 hour interval. A full list of the variables can be seen in [26, Table 3], the variables necessary for this thesis are listed in Table 3.1.

Table 3.1: Variables necessary for this thesis, derived from [26]

Name	Parameter Long Name	Unit	Vertical Levels
hus	Specific Humidity	1	47
ua	Eastward (Zonal) Wind	ms^{-1}	47
va	Westward (Meridional) Wind	ms^{-1}	47
ps	Surface Air Pressure	*Pa*	1
pr	Precipitation	$kg\,m^{-2}s^{-1}$	1

3.2.2 Vertical Hybrid Sigma Pressure Layers

Regarding the vertical levels, all variables were not available in fixed pressure layers but in so called *hybrid sigma pressure coordinates*. In comparison to fixed pressure layers (like 1000 *hPa*, 750 *hPa*...), hybrid sigma pressure coordinates follow the terrain (mountains, valleys etc.). Essentially, sigma vertical levels are given as fractions of the surface pressure P_S at any point, following the equations in [5]:

$$\sigma = h(p, P_S) = \frac{p - P_{top}}{P_S - P_{top}} \tag{3.1}$$

Here $p \in [P_S, P_{top}]$ is a pressure level. It was proposed that instead giving it at pure fractional levels, it would be better to smoothly converge from terrain following fractions

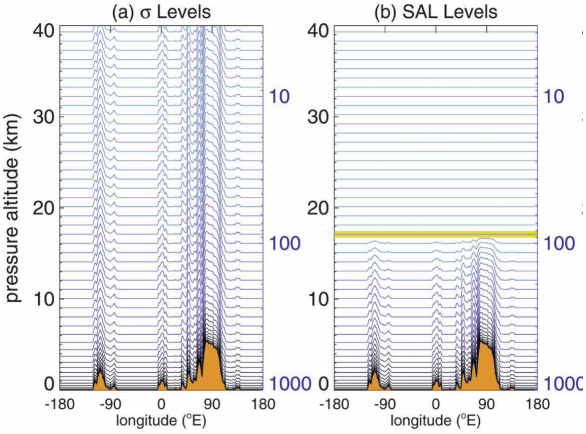

Figure 3.2: Examples of (hybrid) sigma pressure layers. a) shows sigma layers like in Equation 3.1, while b) shows a hybrid approach in the form of Equation 3.2 [5]

(sigma levels) at lower (meaning near the earth surface) levels to isobaric (= same pressure) levels in higher altitudes. This gives numerical as well as practical advantages. So there were alternative functions tested for $h(p, P_S)$, but a final form[1] for calculating pressure levels at any discrete sigma level $\tilde{\eta}$ is

$$p(\tilde{\eta}, P_S) = A(\tilde{\eta}) + B(\tilde{\eta})(P_S - P_{top}) \tag{3.2}$$

with $A(\tilde{\eta})$ being a vertical shift, which is close to 0 at low levels, and $B(\tilde{\eta})$ being a fraction of the pressure range $(P_S - P_{top})$.

This results in levels of equal pressure thickness, converging to isobaric layers at higher altitudes. Which exact form $A(\tilde{\eta})$ and $B(\tilde{\eta})$ took in the MPI GE CMIP6 could not be found in [26], but every dataset using hybrid sigma pressure levels contains the variabels $ap(lev)$, $b(lev)$ and the field of pressure levels $ps(lon, lat, time)$, from which the pressure at any grid-point and level can be calculated with

$$p(lev, lon, lat, time) = ap(lev) + b(lev)ps(lon, lat, time) \tag{3.3}$$

The top pressure can be ignored in this dataset since the upper border is zero.

3.2.3 Structure of the data

The data is available in the HPC cluster of the DKRZ[2], the structure can be seen in if Figure

[1] The equations that lead to to that can be seen in [5]
[2] Deutsches Klimarechenzentrum (en.: German Center for Climate Calculation)

4 Related Work

This section outlies the current state-of-the-art in the main parts of this thesis explained in Section 1.3: Quantifying Moisture (Transport), extracting spatio-temporal patterns, tracking their change over time and visualizing the uncertain results in the end.

4.1 Motivation

As explained in Chapter 1, the approach of this thesis is motivated by the approach of Vietinghoff et al. in [39] and the affiliated dissertation [38], which tackles the issue of detecting critical points in unstable scalar fields. Hereby [39] analyzes the MPI GE [22] from the 5th phase of CMIP, an ensemble simulation with 50 members. The goal was to find the probable centers of pressure high/lows in the NAO pattern (see Section 1.2) and to track their shift over time. They employed a sliding window approach, computing the dominant pattern (see Section 2.2) for each window and member, and determine the likely areas of critical points by merging the results of different memebers per timestep. The centers of mass of these critical areas are then tracked over time to visualize the shift of the pressure high and low. The results show that the patterns do change, and this change is more pronounced if climate change is stronger. Also, there is no significant change if the climate remains stable.

4.2 Moisture Transport

To computationally extract any spatio-temporal patterns of moisture (transport), it first needs to be quantified in any way. The variable from the MPI GE CMIP6 used for this task is the *specific humidity*, which has no unit and is a float value between 0.0 and 1.0, denoting the percentage of water in the air at a specific gridpoint. The vast majority of literature regarding moisture transport use some form of vertically integrated humidity and the variants will be explained in the following section. A popular usage of these

quantifications was to find a filamentary weather structure called "Atmospheric Rivers"[1], a prominent way of water vapor transportation in the extratropic regions [12].

The most straightforward way of quantifying moisture is **Vertically Integrated Water Vapor (IWV)** [2, 12, 23, 33, 43], which is essentially the vertical integral of the specific humidity q over the pressure levels p from earth's surface P_S to some upper limit in the atmosphere:

$$IWV = \frac{1}{g}\int_0^{P_s} q \, \mathrm{d}p \tag{4.1}$$

Similar to Equation 4.1, Zhu and Newell proposed in [45] to use **Vertical Integrated Moisture Transport (IVT)** for Atmospheric River detection. It is calculated by vertically integrating over the different pressure levels the zonal (along latitude lines) and meridional (along longitude lines) fluxes. It became a popular metric for finding atmospheric rivers [12], sometimes alongside IWV [6]. IVT has the unit $\frac{kg}{ms}$ and is usually defined with

$$\overrightarrow{IVT} = \frac{1}{g}\int_0^{P_s} q \begin{pmatrix} u \\ v \end{pmatrix} \mathrm{d}p \tag{4.2}$$

or in a mathematically equivalent form [8]. Here u and v stand for the zonal and meridional components of the horizontal wind vector. While Equation 4.2 yields a vector field, the euclidian norm of said vector field

$$\|IVT\| = \frac{1}{g}\sqrt{(\int_0^{P_s} qu \, \mathrm{d}p)^2 + (\int_0^{P_s} qv \, \mathrm{d}p)^2} \tag{4.3}$$

is also a popular choice in detecting atmospheric rivers [27, 35] and other use cases [1].

The IVT is also part of the atmospheric moisture budget [41] (and similar in [34]) given by

$$\frac{1}{g}\frac{\delta}{\delta t}\int_0^{P_s} q \, \mathrm{d}p = -\nabla \cdot \frac{1}{g}\int_0^{P_s} q \begin{pmatrix} u \\ v \end{pmatrix} \mathrm{d}p + E - P \tag{4.4}$$

With E being the total evaporation and P the precipitation. Yang et al. showed in their report [41] the directions of moisture flux and its evolution in the last three decades. The analysis was done for all continental borders based on the big ERA5 reanalysis. The metrics used for this analysis were mostly the evaporation E, precipitation P and the moisture transport convergence $VIMC = \frac{1}{g}\int_0^{P_s} \nabla \cdot q \begin{pmatrix} u \\ v \end{pmatrix} \mathrm{d}\, p$ from Equation 4.4.

While the integration in the previous equations integrates from the surface to the outer border of the atmosphere (0 Pa), it is quite common to integrate up until the limit of 300

[1] earlier or alternative name: "Tropospheric Rivers"

Table 4.1: Overview table of patterns with moisture transport

Paper ID	Release Year	Pattern extraction	Area of Interest	Timescope	Time Resolution	Studied Season	Variable used for EOF
[36]	2020	SOMs	USA east	1979 to 2017	daily	all year	IVT norm
[1]	2022	EOF	China	1979 to 2010	daily	all year	IVT norm
[30]	1982	EOF	Northern hemishpere	1958 to 1973	monthly/yearly	all year	IWV, IVT_u IVT_v, combined
[8]	2003	EOF	mediterranian sea	1948 to 1996	6hr	DJF	P
[44]	2005	EOF	China	1951 to 1999	monthly	JJA	P
[13]	2018	EOF	USA (west coast)	1948 to 2017	daily	NDJF	IVT norm (assumed)
[16]	2014	EOF	western USA	1979 to 2010	6hr	DJF	IVT norm (assumed)
[47]	2018	EOF	TEIOWP	1961 to 2015	monthly	JJA	IVT
[46]	2020	EOF	TEIOWP	1958 to 2018	6hr/monthly	JJA	Integrated Water Vapor Sink
[42]	2013	EOF	East Asia	1997 to 2002		JJA	IVT_u IVT_v
[18]	2012	EOF	East Asia	1979 to 2009	monthly	summer	IVT

hPa [1, 13, 16, 45], since the amount of moisture in the regions from 300 hPa to 0 Pa is quite neglible and amounts in total to about 2-3 cm/year in terms of freshwater flux [44].

There are also some other notable other algorithms, namely stable oxygen isotope investigation [20] and langragian backwards trajectories [43], but both rather look for the origin of the water vapor instead of its destination and are therefor out of scope for this thesis.

4.3 Pattern analysis regarding IVT

While there are many areas of interest for the application of EOF, this Section will give an overview what kind of pattern analysis has been performed in relation with IVT data. An overview of datasets, timescopes and other metadata is given in Table 4.1.

Although most found related work uses EOF analysis, Teale and Robinson employ an approach using Self Organizing Maps (SOMs) to detect patterns of moisture tronsport in the eastern United States. SOMs are a machine learning approach to reduce data dimensionality, producing a 2D map of higher dimensional data. While they acknowledge the efficiency of EOF to extract dominant patterns, they emphasize the problem of required orthogonality of modes, which is not given for SOMs. The results show that fluxes with the highest moisture content occur less frequently than those with less moisture. But despite the higher moisture content, fluxes with lower moisture transport dominate water vapor movement due to their prevalence. Many of these fluxes meet typical criteria for atmospheric rivers, with varying trajectories and sources suggesting diverse mechanisms of formation. The temporal variability in monthly flux frequencies correlates with regional precipitation patterns, indicating that this approach is a valuable framework for studying precipitation changes [36].

CITE?

Ayantobo et al. analysed the primary six modes of EOF in China, which was grouped in deifferent regions for comparison. While the variances of IVT in eastern to southern

China were quite high, the variances in northern China were quite low. It was shown by comparing the temporal patterns of the primary mode of EOF with the ENSO, that these patterns were related. The cross-wavelet coherence revealed that IVT and ENSO time-series were coherent, which implies that increased IVT was prevalent linked to increased ENSO activities [1].

Published in 1982, Salstein et al. provided the first example of calculating EOF on IVT. Based on data from 91 weather stations, they computed the IVT of the whole northern hemisphere. Statistical siginificance was determined by employing a Monte Carlo testing method. EOF was computed on the IWV, the zonal and meridional IVT fields respectively, but they also evaluated an approach of combining both IVT components in one data vector. They reported the significance of the primary mode of IWV, encoding nearly half (44 %) of variance of the data.

Fernández et al. analyzed the precipitation modes in the mediterranean sea and linking them to the moisture transport in the same area. A goal of this analysis was to contribute to the understanding of the reduction of precipitation which happened in the area as well as to the low-frequency precipitation variability, leading to multiyear drought periods. They employed multiple methods of validating their data: The precipitation data as well as the wind/moisture data for IVT were validated with data from actual weather stations. The stability of the eigenvectors was tested with a Monte Carlo simulation, comparing the variability of actual data with random test data, while degeneracy of the EOF modes was tested using the method of North et al. [24]. Results of the analysis identify the interpretation of the three main precipitation modes: The first mode (22 % variance) seems to be linked to the NAO and Atlantic Storm tracks and associated moisture transports, while the second mode (16 %) represents the internal redistribution of moisture in the mediterranean basin between the estern and western parts. The third mode (11 %) explains increased precipitation in the northern part of the domain. Additionally, moisture transport during positive and negative phases of leading mode showed increased inflow of moisture from the west [8].

Similar to [8], Zhou and Yu analyzed the anoumalous summer rainfall patterns over China and link them to water vapor transport. They confirmed their results by using a second dataset for IVT calculation. They showed that the primary mode of anomalous rainfall is associated with heavier rainfall in the Yangtze river region, while the same applies to the second mode and the Huaihe river. Connecting these patterns to moisture transport, they identified the different ways how these heavier rain areas are coming about by cerain convergences of water vapor transports. Furthermore they compared the supply of

anoumalous rainfall patterns to the one of normal monsoon rainfall, revealing that those differ significantly [44].

In [13], the authors calculate rotated EOF on IVT data and try to analyze the relation between the 15 most dominant modes and the occurence of atmospheric rivers (AR) on the USA west coast. For this they divided the coast into different regions and linked the activity (positive and negative) of the corresponding temporal pattern of each mode to the occurence of atmospheric rivers. It was found that a few modes seem very influational for certain reagions' AR activity, while others seem to play no role at all. They also identfied favorable and unfavorable circulation states (e.g. amongst others a low pressure anomaly in a certain region) for AR occurce [13].

Kim and Alexander showed in their analysis the connection of the IVT patterns in the western USA to three different ENSO events (eastern pacific El Niño (EPEN), central pacific El Niño (CPEN) and La Niña (NINA)). While EPEN events are associated with large positive IVT anomalies from the subtropical Pacific to the north-western USA, CPEN events lead to enhanced moisture transport to the southern USA. During NINA events the mean IVT anomaly is flipped in comparison to EPEN and CPEN. Furthermore it was shown that IVT patterns computed for these events differ significantly from the ones computed for neutral years. Furthermore the results were connected to precipitation anomalies on the USA west coast, showing huge differences (especially for the northern part of the coast) for EPEN and CPEN events. But the authors also emphasize that while the suggestions are strong, exceptions occur (e.g. one El Niño leading to a dry winter, another to the opposite) and need to be studied in greater detail.

Similar to [39] and the approach of this thesis, Zou et al. applied a sliding window approach to IVT patterns in the tropical Indian Ocean–western Pacific to analyze the evolution over time. For the studied period from 1961 to 2015, they studied every 20 year period with a 5 year sliding window, computing Multivariate EOFs for each window, resulting in vector fields of patterns. The results show that the two most significant modes show significant changes in the mid 80s: The primary mode is characterized by a anti-cyclonic pattern in the north-western Pacific, which shifts significantly to the south. An analysis of the relation to sea surface temperature (SST) revealed that the correlation between the mode and SST rose in the mid 80s, from weakly correlated to significant positive correlation between IVT and SST anomalies. Furthermore, the primary mode seems to be regulated significantly bei ENSO. The second most significant mode is related to the variablility of the tropical Indian Ocean dipole (defined by the differences in average SST) [47].

A different approach was employed by [46], evaluating the EOF patterns of vertically integrated apparent moisture sink. Results indicate that the primary mode is a southwest-

northeast oriented dipole, while the secondary mode is a southwest-northeast oriented tripole. The primary mode seems to be heavily regulated by the ENSO in the previous winter season, while the second mode seems to originates from internal atmopheric variability. Based on the much higher standard deviations in ENSO years, it seems that water vapor source and sink tend to be dominated by the primary mode in ENSO years, while the secondary mode is prevalent in non-ENSO years.

While the main focus of [42] is to evaluate and compare a regional air-sea coupled model, they also performed EOF analysis on the zonal and meridional components of IVT, respectively. They used the results to evaluate the connection to SST, revealing that the results from the regional coupled model aligns better with results from other datasets and reality than the regional uncoupled model.

Li and Zhou evaluated the connection of the IVT-EOF patterns to ENSO in the asian western northern Pacific. They used a different approach then most in applying EOF to IVT, by concatenating the meridional and zonal components in one matrix and calculating EOF on it. To confirm their results, they compared the results with another reanalysis from the same (and a larger) region. Furthermore, these IVT patterns were linked to the SST. They revealed the characteristics of the two most significant modes, but most prominently they showed the quasi-4-year coupling of the two most prominent modes with ENSO [18].

4.4 Uncertainity Visualisation

Since the used dataset (see Chapter 3) is an ensemble simulation consisting of 50 members, most of the figures and other visual representations in this thesis need to display the uncertainity stemming from them. This section summarizes advances fitting for this topic, giving a frame of references of current possibilities of vizualizing uncertainity.

Kamal et al. give a recent overview over the whole topic of uncertainity visualization: From the introduction to the whole concept of uncertainity, to the differentiation between different kinds of uncertainity in the visualisation process. They grouped all kinds of representing uncertainity in two categories: quatification, consisting of mostly mathematical approaches of handling uncertain data, and visualisation, displaying the uncertain data in a way directly. An overview of the different kinds of uncertainity visualization were given: Manipulation of attributes (like shading), animation, visual variables (like color, hue, brightness), graphical techniques like box/scatter plots and glyphs. Furthermore, recent advances in uncertainity visualization are given, with a special emphasis on ensemble (simulation) data, big data and machine learning, listing the most prominent areas where the presentation of uncertainity is crucial. In the end, a framework for evaluating un-

certainity visualization is presented, followed by an overview of possible future research directions [15].

A way of using animation to display uncertainity in scalar fields was shown by Coninx et al. Their goal was to enrich the usual display of scalar fields with colormaps with additional uncertainity information. The tool of choice here was animated Perlin noise, and the uncertainity was presented by modifying the noise mask with the uncertainity information at each point. The results were tested using a psychophysical evaluation of contrast sensitivity thresholds [4], evaluating effective parameters for proper presentation of the uncertain area [4].

Sanyal et al. proposed Noodles, a tool for displaying uncertainity in weather ensemble simulations. It employs three different ways of displaying uncertain isocontours: ribbon, glyphs and spaghetti plots. Additionally, they added tools for exploring the uncertainity of datasets, like an colormap of the whole dataset uncertainity. Uncertainity in spaghetti plots is clear (one line per member), but gets confusing and chaotic quickly. The glyphs display the uncertainity by different sizes, and can be displayed on the whole map or alogside means of isocontours. Ribbons condense the information of multiple lines by adapting the ribbon width to the uncertainity of isolines at a specific gridpoint. The resulting tool was tested by two meteorologists, and classified the results as beneficial [31].

Another way of visualizing groups of isocontours are contour boxplots proposed in [40], grouping isocontours together in a similar way like conventional boxplots. This means that the easiest default presentation (spaghetti plots) is replaced by popular boxplot stats: The median, the mean, the quartiles around that mean, the whole range and the outliers (not part of the whole range). But the implementation is not as straight forward as in conventional boxplots. To quantify the aforementioned statistics, Whitaker et al. propose a data depth based approach, which encodes how much a particular sample is centrally located in its function (or in this case: How central is a isocontour to a whole set of isocontours). While the results look very promising, it lacks a publicly available implementation, making it hard to use the approach.

5 Methodology

5.1 Overview

Explain what I want to do using the CMIP6 simulations: Describe what the general plan is: Visualisation of the moisture transport in Europe with the help . Also define what the goals of the visualisations are: Visualize different scenarios for comparison, visualize uncertainties of different members, visualize evolution over time, also try combining those. Here should be a graphic that explains the workflow that transforms a simulation into some nice pictures

5.2 Preprocessing

The goal of this step is to prepare the data for further usage. One main goal is to reduce the size, so first of all the geographic region of interest is cut out, which is the Northern Atlantic (derived from [39]): $-90^{\circ}W - 40^{\circ}E$, $20^{\circ} - 80^{\circ}N$. For the compared variables (precipitation, surface pressure) the preprocessing is already done, but in case of IVT it still needs to be calculated.

1. Load four different fields for each time period in each member in each szenario: Specific humidity *hus*, eastward horizontal wind *ua*, northward horizontal wind *va* and surface pressure *ps*. Here the geographical box around the area of interest is cut out: Europe and the North Atlantic (Longitude: $-90 \longrightarrow 40$, Latitude: $20 \longrightarrow 80$, based on [39])

2. For each geographical gridpoint (*lon*, *lat*) and timestep: Calculate the integrals of hte product of wind components and specific humidity over the vertical pressure levels $\frac{1}{g}\int_{p_S}^{0} hus * ua$ and $\frac{1}{g}\int_{p_S}^{0} hus * va$, with g being the gravitational acceleration ($9.806\frac{m}{s}$)

3. Save the results for each time period in each member in each szenario in a NetCDF file for the further steps.

The calculations were performed on the high performance computing cluster[1] of the German Climate Calculations Center (DKRZ), due to the MPI GE CMIP6 is saved there and downloading the data would take a lot of time. This also result in the goal of this step to minimize the hours on the HPC system since they get billed by the time using nodes. Although these steps seem easy, due to the large sizes of the datasets and other issues many challenges were met. In the following those will be explained with regard to the step they ocurred in.

1. Data Loading

- cutting out geobox
- slow IO ⟶ started using dask+xarray

2. Vertical integration

- calculate hybrid sigma pressure levels for each gridpoint and timestep to get the x values for integration
- describe my idea of testing the integration

5.2.1 Problems with Preprocessing

The steps described in the section before were just the final attempt. The first (and many following) coding versions were implemented in Julia [11], using just a NetCDF library[2] while the rest was coded from scratch. The algorithm was very simple:

1. Load all datasets into the RAM (as recommended by the NetCDF library itself) and cut out the used gegraphical limits. This should be feasible since all in all one dataset for one timescope-file accounts for $\tilde{1}2$ GB[3], so the maximum is around 36 GB, since the surface pressure data is not that large (260 MB)
2. Calculate the IVT with trapezoidial integration multithreaded by handling one timestep by one thread
3. Write the results (euklidian norm and the meridional/zonal component)

Although julia promises high performance, it performed quite poorly on the HPC. The reason for this is the slow IO on the cluster: While the calculation itself took only $\tilde{2}35$ s

[1] https://docs.dkrz.de/doc/levante/
[2] https://alexander-barth.github.io/NCDatasets.jl/stable/
[3] $70\ lon * 32\ lat * 47\ levels * 29220\ timesteps * 4\ byte \approx 12GB$

($\approx 4\,min$)[4], the loading of the required datasets took around $\tilde{3}350s$ ($\approx 55\,min$). This results in roughly $5h$ (including saving the data to disk) for one member of ScenarioMIP, which leads to $250h$ node hours for one scenario. Taking into account that it needs to run for historical simulations as well as other scenarios, this was not feasible according to the limited node hours provided[5].

To reduce the loading time of the data multiple optimizations were evaluated. First of all reducing the amount of

[4] Refering here and in the following to one timescope of 20 years in one member
[5] Also taking into account that the processes may need to run multiple times due to errors

6 Results

7 Conclusions and Future Work

7.1 Conclusions

7.2 Future Work

Bibliography

1. O. O. Ayantobo, J. Wei, B. Kang, and G. Wang. "Integrated moisture transport variability over China: patterns, impacts, and relationship with El Nino–Southern Oscillation (ENSO)". en. *Theoretical and Applied Climatology* 147:3-4, 2022, pp. 985–1002. ISSN: 0177-798X, 1434-4483. DOI: 10.1007/s00704-021-03864-x.

2. J.-W. Bao, S. A. Michelson, P. J. Neiman, F. M. Ralph, and J. M. Wilczak. "Interpretation of Enhanced Integrated Water Vapor Bands Associated with Extratropical Cyclones: Their Formation and Connection to Tropical Moisture". en. *Monthly Weather Review* 134:4, 2006, pp. 1063–1080. ISSN: 1520-0493, 0027-0644. DOI: 10.1175/MWR3123.1.

3. M. Böttinger and D. D. Kasang. *The SSP Scenarios*. en. Page.

4. A. Coninx, G.-P. Bonneau, J. Droulez, and G. Thibault. "Visualization of uncertain scalar data fields using color scales and perceptually adapted noise". en. In: *Proceedings of the ACM SIGGRAPH Symposium on Applied Perception in Graphics and Visualization*. ACM, Toulouse France, 2011, pp. 59–66. ISBN: 978-1-4503-0889-2. DOI: 10.1145/2077451.2077462.

5. S. Eckermann. "Hybrid σ–p Coordinate Choices for a Global Model". EN. *Monthly Weather Review* 137:1, 2009. Publisher: American Meteorological Society Section: Monthly Weather Review, pp. 224–245. ISSN: 1520-0493, 0027-0644. DOI: 10.1175/2008MWR2537.1.

6. J. Eiras-Barca, S. Brands, and G. Miguez-Macho. "Seasonal variations in North Atlantic atmospheric river activity and associations with anomalous precipitation over the Iberian Atlantic Margin". en. *Journal of Geophysical Research: Atmospheres* 121:2, 2016. _eprint: https://onlinelibrary.wiley.com/doi/pdf/10.1002/2015JD023379, pp. 931–948. ISSN: 2169-8996. DOI: 10.1002/2015JD023379.

7. V. Eyring, S. Bony, G. A. Meehl, C. A. Senior, B. Stevens, R. J. Stouffer, and K. E. Taylor. "Overview of the Coupled Model Intercomparison Project Phase 6 (CMIP6) experimental design and organization". en. *Geoscientific Model Development* 9:5, 2016, pp. 1937–1958. ISSN: 1991-9603. DOI: 10.5194/gmd-9-1937-2016.

8. J. Fernández, J. Sáenz, and E. Zorita. "Analysis of wintertime atmospheric moisture transport and its variability over southern Europe in the NCEP Reanalyses". en. *Climate Research* 23, 2003, pp. 195–215. ISSN: 0936-577X, 1616-1572. DOI: 10.3354/cr023195.

9. E. Foote. "Circumstances affecting the heat of the sun's rays". *Am. J. Sci. Arts* 22:66, 1856, pp. 383–384.

10. J. Fourier. "Remarques générales sur les températures du globe terrestre et des espaces planétaires". In: *Annales de Chemie et de Physique*. Vol. 27. 1824, pp. 136–167.

11. K. Gao, G. Mei, F. Piccialli, S. Cuomo, J. Tu, and Z. Huo. "Julia language in machine learning: Algorithms, applications, and open issues". *Computer Science Review* 37, 2020, p. 100254. ISSN: 1574-0137. DOI: 10.1016/j.cosrev.2020.100254.

12. L. Gimeno, R. Nieto, M. Vázquez, and D. Lavers. "Atmospheric rivers: a mini-review". *Frontiers in Earth Science* 2, 2014. ISSN: 2296-6463.

13. K. Guirguis, A. Gershunov, R. E. S. Clemesha, T. Shulgina, A. C. Subramanian, and F. M. Ralph. "Circulation Drivers of Atmospheric Rivers at the North American West Coast". en. *Geophysical Research Letters* 45:22, 2018. _eprint: https://onlinelibrary.wiley.com/doi/pdf/10.1029/2018GL079249, pp. 12, 576–12, 584. ISSN: 1944-8007. DOI: 10.1029/2018GL079249.

14. Intergovernmental Panel On Climate Change (Ipcc). *Climate Change 2021 – The Physical Science Basis: Working Group I Contribution to the Sixth Assessment Report of the Intergovernmental Panel on Climate Change*. en. 1st ed. Cambridge University Press, 2023. ISBN: 978-1-00-915789-6. DOI: 10.1017/9781009157896.

15. A. Kamal, P. Dhakal, A. Y. Javaid, V. K. Devabhaktuni, D. Kaur, J. Zaientz, and R. Marinier. "Recent advances and challenges in uncertainty visualization: a survey". en. *Journal of Visualization* 24:5, 2021, pp. 861–890. ISSN: 1343-8875, 1875-8975. DOI: 10.1007/s12650-021-00755-1.

16. H.-M. Kim and M. A. Alexander. "ENSO's Modulation of Water Vapor Transport over the Pacific–North American Region". en. *Journal of Climate* 28:9, 2015, pp. 3846–3856. ISSN: 0894-8755, 1520-0442. DOI: 10.1175/JCLI-D-14-00725.1.

17. H. Lee, K. Calvin, D. Dasgupta, G. Krinner, A. Mukherji, P. Thorne, C. Trisos, J. Romero, P. Aldunce, and A. C. Ruane. "Climate change 2023 synthesis report summary for policymakers". *CLIMATE CHANGE 2023 Synthesis Report: Summary for Policymakers*, 2024.

18. X. Li and W. Zhou. "Quasi-4-Yr Coupling between El Niño–Southern Oscillation and Water Vapor Transport over East Asia–WNP". en. *Journal of Climate* 25:17, 2012, pp. 5879–5891. ISSN: 0894-8755, 1520-0442. DOI: 10.1175/JCLI-D-11-00433.1.

19. D. Lobelle, C. Beaulieu, V. Livina, F. Sévellec, and E. Frajka-Williams. "Detectability of an AMOC Decline in Current and Projected Climate Changes". en. *Geophysical Research Letters* 47:20, 2020. _eprint: https://onlinelibrary.wiley.com/doi/pdf/10.1029/2020GL089974, e2020GL089974. ISSN: 1944-8007. DOI: 10.1029/2020GL089974.

20. Y. Ma, M. Lu, H. Chen, M. Pan, and Y. Hong. "Atmospheric moisture transport versus precipitation across the Tibetan Plateau: a mini-review and current challenges". en.

21. N. Maher, S. Milinski, and R. Ludwig. "Large ensemble climate model simulations: introduction, overview, and future prospects for utilising multiple types of large ensemble". en. *Earth System Dynamics* 12:2, 2021, pp. 401–418. ISSN: 2190-4987. DOI: 10.5194/esd-12-401-2021.

22. N. Maher, S. Milinski, L. Suarez-Gutierrez, M. Botzet, M. Dobrynin, L. Kornblueh, J. Kröger, Y. Takano, R. Ghosh, C. Hedemann, C. Li, H. Li, E. Manzini, D. Notz, D. Putrasahan, L. Boysen, M. Claussen, T. Ilyina, D. Olonscheck, T. Raddatz, B. Stevens, and J. Marotzke. "The Max Planck Institute Grand Ensemble: Enabling the Exploration of Climate System Variability". en. *Journal of Advances in Modeling Earth Systems* 11:7, 2019, pp. 2050–2069. ISSN: 1942-2466, 1942-2466. DOI: 10.1029/2019MS001639.

23. P. J. Neiman, F. M. Ralph, G. A. Wick, J. D. Lundquist, and M. D. Dettinger. "Meteorological Characteristics and Overland Precipitation Impacts of Atmospheric Rivers Affecting the West Coast of North America Based on Eight Years of SSM/I Satellite Observations". en. *Journal of Hydrometeorology* 9:1, 2008, pp. 22–47. ISSN: 1525-7541, 1525-755X. DOI: 10.1175/2007JHM855.1.

24. G. R. North, T. L. Bell, R. F. Cahalan, and F. J. Moeng. "Sampling Errors in the Estimation of Empirical Orthogonal Functions". EN. *Monthly Weather Review* 110:7, 1982. Publisher: American Meteorological Society Section: Monthly Weather Review, pp. 699–706. ISSN: 1520-0493, 0027-0644. DOI: 10.1175/1520-0493(1982)110<0699:SEITEO>2.0.CO;2.

25. B. C. O'Neill, C. Tebaldi, D. P. Van Vuuren, V. Eyring, P. Friedlingstein, G. Hurtt, R. Knutti, E. Kriegler, J.-F. Lamarque, J. Lowe, G. A. Meehl, R. Moss, K. Riahi, and B. M. Sanderson. "The Scenario Model Intercomparison Project (ScenarioMIP) for CMIP6". en. *Geoscientific Model Development* 9:9, 2016, pp. 3461–3482. ISSN: 1991-9603. DOI: 10.5194/gmd-9-3461-2016.

26. D. Olonscheck, L. Suarez-Gutierrez, S. Milinski, G. Beobide-Arsuaga, J. Baehr, F. Fröb, L. Hellmich, T. Ilyina, C. Kadow, D. Krieger, H. Li, J. Marotzke, É. Plésiat, M. Schupfner, F. Wachsmann, K.-H. Wieners, and S. Brune. *The new Max Planck Institute Grand Ensemble with CMIP6 forcing and high-frequency model output*. en. preprint. Preprints, 2023. DOI: 10.22541/essoar.168319746.64037439/v1.

27. A. M. Ramos, R. Nieto, R. Tomé, L. Gimeno, R. M. Trigo, M. L. R. Liberato, and D. A. Lavers. "Atmospheric rivers moisture sources from a Lagrangian perspective". en. *Earth System Dynamics* 7:2, 2016, pp. 371–384. ISSN: 2190-4987. DOI: 10.5194/esd-7-371-2016.

28. K. Riahi, D. P. Van Vuuren, E. Kriegler, J. Edmonds, B. C. O'Neill, S. Fujimori, N. Bauer, K. Calvin, R. Dellink, O. Fricko, W. Lutz, A. Popp, J. C. Cuaresma, S. Kc, M. Leimbach, L. Jiang, T. Kram, S. Rao, J. Emmerling, K. Ebi, T. Hasegawa, P. Havlik, F. Humpenöder, L. A. Da Silva, S. Smith, E. Stehfest, V. Bosetti, J. Eom, D. Gernaat, T. Masui, J. Rogelj, J. Strefler, L. Drouet, V. Krey, G. Luderer, M. Harmsen, K. Takahashi, L. Baumstark, J. C. Doelman, M. Kainuma, Z. Klimont, G. Marangoni, H. Lotze-Campen, M. Obersteiner, A. Tabeau, and M. Tavoni. "The Shared Socioeconomic Pathways and their energy, land use, and greenhouse gas emissions implications: An overview". en. *Global Environmental Change* 42, 2017, pp. 153–168. ISSN: 09593780. DOI: 10.1016/j.gloenvcha.2016.05.009.

29. W. J. Ripple, C. Wolf, T. M. Newsome, P. Barnard, and W. R. Moomaw. "World Scientists' Warning of a Climate Emergency". en. *BioScience*, 2019, biz088. ISSN: 0006-3568, 1525-3244. DOI: 10.1093/biosci/biz088.

30. D. A. Salstein, R. D. Rosen, and J. P. Peixoto. "Modes of Variability in Annual Hemispheric Water Vapor and Transport Fields". en. *Journal of the Atmospheric Sciences* 40:3, 1983, pp. 788–804. ISSN: 0022-4928, 1520-0469. DOI: 10.1175/1520-0469(1983)040<0788:MOVIAH>2.0.CO;2.

31. J. Sanyal, Song Zhang, J. Dyer, A. Mercer, P. Amburn, and R. J. Moorhead. "Noodles: A Tool for Visualization of Numerical Weather Model Ensemble Uncertainty". en. *IEEE Transactions on Visualization and Computer Graphics* 16:6, 2010, pp. 1421–1430. ISSN: 1077-2626. DOI: 10.1109/TVCG.2010.181.

32. J. S. Sawyer. "Man-made carbon dioxide and the "greenhouse" effect". *Nature* 239:5366, 1972, pp. 23–26.

33. P. Schluessel and W. J. Emery. “Atmospheric water vapour over oceans from SSM/I measurements”. en. *International Journal of Remote Sensing* 11:5, 1990, pp. 753–766. ISSN: 0143-1161, 1366-5901. DOI: 10.1080/01431169008955055.

34. R. Seager, H. Liu, Y. Kushnir, T. J. Osborn, I. R. Simpson, C. R. Kelley, and J. Nakamura. “Mechanisms of Winter Precipitation Variability in the European–Mediterranean Region Associated with the North Atlantic Oscillation”. en. *Journal of Climate* 33:16, 2020, pp. 7179–7196. ISSN: 0894-8755, 1520-0442. DOI: 10.1175/JCLI-D-20-0011.1.

35. P. M. Sousa, A. M. Ramos, C. C. Raible, M. Messmer, R. Tomé, J. G. Pinto, and R. M. Trigo. “North Atlantic Integrated Water Vapor Transport—From 850 to 2100 CE: Impacts on Western European Rainfall”. en. *Journal of Climate* 33:1, 2020, pp. 263–279. ISSN: 0894-8755, 1520-0442. DOI: 10.1175/JCLI-D-19-0348.1.

36. N. Teale and D. A. Robinson. “Patterns of Water Vapor Transport in the Eastern United States”. *Journal of Hydrometeorology* 21:9, 2020, pp. 2123–2138. ISSN: 1525-755X, 1525-7541. DOI: 10.1175/JHM-D-19-0267.1.

37. L. Touzé-Peiffer, A. Barberousse, and H. Le Treut. “The Coupled Model Intercomparison Project: History, uses, and structural effects on climate research”. en. *WIREs Climate Change* 11:4, 2020, e648. ISSN: 1757-7780, 1757-7799. DOI: 10.1002/wcc.648.

38. D. Vietinghoff. “Critical Points of Uncertain Scalar Fields”, 2024.

39. D. Vietinghoff, C. Heine, M. Bottinger, N. Maher, J. Jungclaus, and G. Scheuermann. “Visual Analysis of Spatio-Temporal Trends in Time-Dependent Ensemble Data Sets on the Example of the North Atlantic Oscillation”. en. In: *2021 IEEE 14th Pacific Visualization Symposium (PacificVis)*. IEEE, Tianjin, China, 2021, pp. 71–80. ISBN: 978-1-66543-931-2. DOI: 10.1109/PacificVis52677.2021.00017.

40. R. T. Whitaker, M. Mirzargar, and R. M. Kirby. “Contour Boxplots: A Method for Characterizing Uncertainty in Feature Sets from Simulation Ensembles”. *IEEE Transactions on Visualization and Computer Graphics* 19:12, 2013, pp. 2713–2722. ISSN: 1077-2626. DOI: 10.1109/TVCG.2013.143.

41. Y. Yang, C. Liu, N. Ou, X. Liao, N. Cao, N. Chen, L. Jin, R. Zheng, K. Yang, and Q. Su. “Moisture Transport and Contribution to the Continental Precipitation”. en. *Atmosphere* 13:10, 2022, p. 1694. ISSN: 2073-4433. DOI: 10.3390/atmos13101694.

42. S. Yao, Q. Huang, Y. Zhang, and X. Zhou. “The simulation of water vapor transport in East Asia using a regional air–sea coupled model”. en. *Journal of Geophysical Research: Atmospheres* 118:4, 2013, pp. 1585–1600. ISSN: 2169-897X, 2169-8996. DOI: 10.1002/jgrd.50089.

43. N. Zhao, A. Manda, X. Guo, K. Kikuchi, T. Nasuno, M. Nakano, Y. Zhang, and B. Wang. "A Lagrangian View of Moisture Transport Related to the Heavy Rainfall of July 2020 in Japan: Importance of the Moistening Over the Subtropical Regions". en. *Geophysical Research Letters* 48:5, 2021, e2020GL091441. ISSN: 0094-8276, 1944-8007. DOI: 10.1029/2020GL091441.

44. T.-J. Zhou and R.-C. Yu. "Atmospheric water vapor transport associated with typical anomalous summer rainfall patterns in China". en. *Journal of Geophysical Research: Atmospheres* 110:D8, 2005, 2004JD005413. ISSN: 0148-0227. DOI: 10.1029/2004JD005413.

45. Y. Zhu and R. E. Newell. "A Proposed Algorithm for Moisture Fluxes from Atmospheric Rivers". en. *Monthly Weather Review* 126:3, 1998, pp. 725–735. ISSN: 0027-0644, 1520-0493. DOI: 10.1175/1520-0493(1998)126<0725:APAFMF>2.0.CO;2.

46. M. Zou, S. Qiao, L. Chao, D. Chen, C. Hu, Q. Li, and G. Feng. "Investigating the Interannual Variability of the Boreal Summer Water Vapor Source and Sink over the Tropical Eastern Indian Ocean-Western Pacific". en. *Atmosphere* 11:7, 2020, p. 758. ISSN: 2073-4433. DOI: 10.3390/atmos11070758.

47. M. Zou, S. Qiao, T. Feng, Y. Wu, and G. Feng. "The inter-decadal change in anomalous summertime water vapour transport modes over the tropical Indian Ocean–western Pacific in the mid-1980s". en. *International Journal of Climatology* 38:6, 2018, pp. 2672–2685. ISSN: 0899-8418, 1097-0088. DOI: 10.1002/joc.5452.